Engineering Pt-Bi₂O₃ Interface to Boost Cyclohexanone Selectivity in Oxidative Dehydrogenation of KA-Oil

Qiuyue Zhou [1,†], Zhi-Qiang Wang [2,*,†], Wei Hong [1], Baohui Lou [1] and Shihui Zou [1,*]

1. Key Lab of Applied Chemistry of Zhejiang Province, Department of Chemistry, Zhejiang University, Hangzhou 310036, China; 21737080@zju.edu.cn (Q.Z.); 11437031@zju.edu.cn (W.H.); 11937004@zju.edu.cn (B.L.)
2. Key Laboratory for Advanced Materials and Joint International Research Laboratory for Precision Chemistry and Molecular Engineering, Feringa Nobel Prize Scientist Joint Research Center, Centre for Computational Chemistry and Research Institute of Industrial Catalysis, School of Chemistry and Molecular Engineering, East China University of Science and Technology, Shanghai 200237, China
* Correspondence: zhiqiangwang@ecust.edu.cn (Z.-Q.W.); xueshan199@zju.edu.cn (S.Z.)
† These authors contributed equally to this work.

Abstract: Oxidative dehydrogenation of KA-oil (a mixture of cyclohexanone and cyclohexanol) is an economically attractive process to produce cyclohexanone because it provides a chance to avoid the energy-intensive alcohol-ketone separation process. The application of this process, however, is hampered by the low cyclohexanone selectivity which results from the competitive adsorption of cyclohexanol and cyclohexanone on the catalyst surface. Herein, by engineering Pt-Bi₂O₃ interface to tune the geometric and electronic structure of Pt, we successfully weaken the cyclohexanone adsorption without compromising the oxidation of cyclohexanol. As a result, Bi₂O₃-Pt/SiO₂ with Bi-to-Pd ratio of 0.2 exhibits a 5 times higher cyclohexanone selectivity than Pt/SiO₂ at the same conversion of KA oil. Long term test suggests that the Pt-Bi₂O₃ interface is stable in the oxidative dehydrogenation of KA-oil.

Keywords: KA-oil; oxidative dehydrogenation; bismuth; Pt; electronic effect

1. Introduction

Cyclohexanone is recognized as an important industrial feedstock to produce caprolactam and adipic acid, which are key intermediates in the manufacture of nylon 6 and nylon 66 [1–3]. Industrially, nearly 90% of cyclohexanone is manufactured in the form of KA-oil through the process of selective oxidation of cyclohexane. Cyclohexanol separated from KA-oil can also be used to produce cyclohexanone through an endothermic anaerobic dehydrogenation process, but the single-pass yield is limited by thermodynamic equilibrium (50–60%), which again produces KA-oil [4,5]. In order to obtain pure cyclohexanone, tedious steps of distillation separation and purification are indispensable. These steps are energy-intensive and pollutive because the boiling points of cyclohexanol (161 °C) and cyclohexanone (155 °C) are very close [6,7]. For the purpose of simplifying operation and saving energy, it is appealing to develop an oxidative dehydrogenation (ODH) process of KA-oil (Scheme 1) with potential 100% yield of cyclohexanone [8]. Nevertheless, no catalysts have been reported to reach this target yet. Even if pure cyclohexanol is used as the substrate, the conversion is usually less than 80% [9–12]. The biggest challenge in the ODH of KA-oil is the competitive adsorption between ketone and alcohol, which results in low alcohol conversion and non-ideal ketone selectivity. To address this problem, it is of great importance to develop advanced catalysts that feature a weak adsorption of cyclohexanone but have a strong adsorption of cyclohexanol
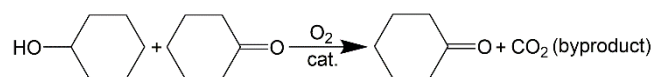
Scheme 1. Reaction route of catalytic oxidative dehydrogenation of KA-oil.

The adsorption behavior of heterogeneous catalysts is generally determined by their surface geometric and electronic structures [13–15]. For a structure-sensitive reaction, different crystal planes might exhibit different adsorption behaviors towards reactants and products. In this situation, engineering the morphology and exposed crystal planes of nanoparticles can regulate the adsorption behavior to optimize the catalytic performance. For example, Hong et al. reported a precise geometric control over Pt nanoparticles (PtNPs) by tuning the calcination atmosphere. They demonstrated that cubic PtNPs possessed stronger adsorption towards cyclohexanol than octahedral PtNPs and thus displayed better catalytic activity in oxidation of KA-oil [13]. Zhou et al. reported solvent post-treatment as an efficient process to manipulate the crossover of Au nanoparticles between multiply twinned nanoparticle (MTP) and single crystal. They found that twin boundaries exposed with {211}-like facets can significantly enhance the chemisorption of alcohol molecules and therefore greatly improve the ODH of alcohols [16]. In addition, introducing second component to block part of active sites might provide different substrate coordination route that in turn modify the activity and the selectivity of the original catalyst [17]. For example, Villa et al. reported that the addition of Bi into PdAu/C can significantly improve the selectivity in ODH of benzyl alcohol because Bi blocks partial of active sites and suppress parallel reaction in ODH of benzyl alcohol [18]. In addition to geometric effect, creating metal-metal [15,19], metal-support [20] or metal-organic interfaces [14] to tune the electronic structures of metal nanoparticles is also an important strategy to regulate their adsorption behaviors. Among them, p-electron metal Bi, is frequently used as a modifier to engineer the electronic structure of Pd and Pt as it can donate electrons to these active species and prevent them from being overoxidized [21,22]. However, the promoting effect of Bi is usually reported in the low-temperature liquid-phase oxidation of alcohols. Limited progress is reported in high-temperature gas-phase ODH of alcohols. Conventional studies usually use relatively high loading of metallic Bi. The promoting effect of the very low loading of Bi_2O_3 is rarely reported.

Here, we systematically studied the promoting effect of bismuth oxide in Pt-catalyzed gas-phase ODH of KA-oil. We found that grafting a small amount of Bi_2O_3 onto PtNPs can significantly improve the cyclohexanone selectivity without compromising of cyclohexanol conversion. Kinetic studies and characterizations suggested that the engineered Pt-Bi_2O_3 interface altered the geometric and electronic structure of Pt, which resulted in weaker adsorption of cyclohexanone and thus prevented it from over-oxidizing to CO_2.

2. Results

Bi is a well-known promoter for Pt catalysts in alcohol oxidation [21]. The origin of the promoting effect, however, is still under debate [22]. Mondelli et al. suggested that metallic Bi can prevent active Pt species from being overoxidized [23]. Mallat et al. ascribed the promoting effect of Bi to the geometric blocking of poisonous intermediates on Pt particles [24]. Zhou et al. [25] believed that strong synergic interaction between partially oxidized BiO_x and Pt made the major contribution to the promotion. To date, it remains a question whether Bi in totally oxidized form (i.e., Bi_2O_3) can still promote the Pt-catalyzed ODH of alcohols. To answer this question, we first performed density functional theory (DFT) calculations over Pt(111) and Bi_2O_3 modified Pt(111) surfaces considering that (111) is the most stable surface of Pt (Figure 1). The structure of Bi_2O_3-Pt(111) was built by the genetic algorithm optimization method inside the USPEX crystal structure prediction software, which has been successfully applied in the prediction of stable structure of massive crystals, nanoclusters, and reconstructed crystal surface [26,27]. Bader charge analysis suggests that the Pt on Bi_2O_3-Pt(111) is -0.168 |e| while that for Bi_2O_3 is $+0.168$ |e|, indicating the electron transfer towards Pt across the Bi_2O_3/Pt interface. Interestingly,

the modification of surface electronic structure as well as the inherent geometric blocking effect eventually changes the adsorption energy of Pt towards cyclohexanone. As can be seen from Figure 1, the adsorption energy of the most stable binding configuration for cyclohexanone on Pt(111) is 1.02 eV, whereas this value decreases to 0.67 eV after Bi_2O_3 modification. These results therefore predicted Pt- Bi_2O_3 interface engineering as an effective strategy to regulate the adsorption of cyclohexanone, which is closely related to the performance of the ODH of KA-oil.
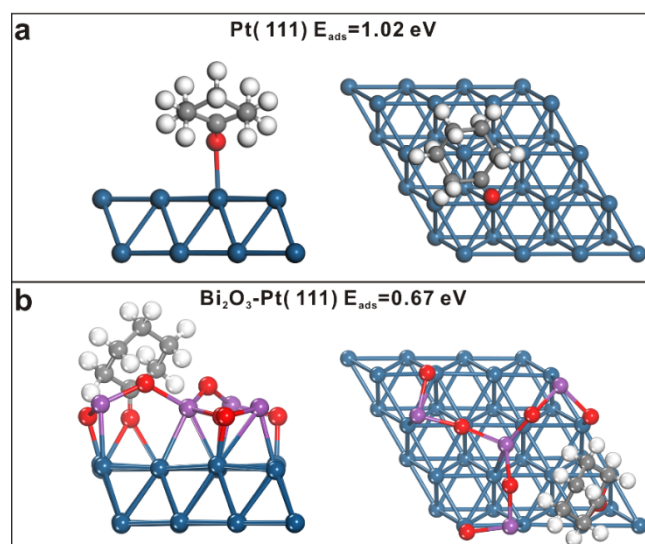

Figure 1. Calculated structures and the adsorption energies of the cyclohexanone on (**a**) Pt(111) and (**b**) Bi_2O_3 modified Pt(111). Pt, Bi, C, O, and H atoms are in blue, purple, gray, red, and white, respectively. The results of Pt(111) is consistent with our previous work and is reproduced with permission from [13]. Copyright 2018, Wiley-VCH.

It has been reported that small Pt nanoparticles (2–5 nm in diameter) exhibited excellent catalytic performances in the aerobic oxidation of KA-oil [8].Directed by the literature and our theoretical results, we synthesized $PtBi/SiO_2$ materials by a wet impregnation method using bismuth nitrate and Pt nanoparticles (~3 nm) [28] as precursors. The loading amount of Pt was fixed as 1 wt.% while the mass ratio of Bi-to-Pt varied from 0.05 to 0.3. As shown in Figure 2, the average size of Pt particles remains 3–4 nm regardless of the bismuth content, suggesting the adding of Bi did not significantly change the particle size of Pt. It has been reported that surface structure of Pt nanoparticles within 5 nm are usually similar, with the exposure of low index surfaces [29]. HRTEM images of $PtBi_{0.2}/SiO_2$ (Figure 3a,b) depicted characteristic spacing of 0.227 nm for Pt (111) surfaces. The corresponding FFT pattern indicated that the nanoparticles are single crystals. Elemental mappings of $PtBi_{0.2}/SiO_2$ (Figure 3d,e) showed that the detected Bi signals generally located around Pt signals, which means that the introduced bismuth species preferred to graft onto Pt nanoparticles. The observation is in line with that of Ning et al., who found the selective adsorption of Bi on or near PtNPs when introducing bismuth precursor to carbon nanotubes supported Pt material by impregnation [30]. XRD patterns in Figure 4a showed that diffraction peak of Pt (111) did not show any deviation after the introduction of Bi, implying the absence of Pt-Bi alloy after the thermal calcination in air. No diffraction peak related to Bi was observed because the loading amount is very low [25,31].
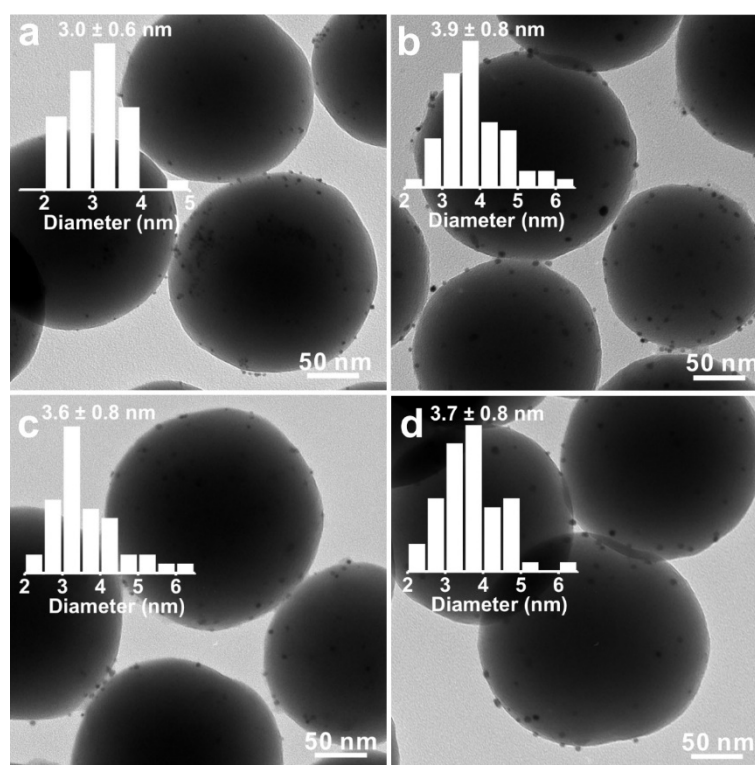
Figure 2. TEM images of Pt/SiO$_2$ and PtBi$_x$/SiO$_2$, (**a**) Pt/SiO$_2$, (**b**) PtBi$_{0.05}$/SiO$_2$, (**c**) PtBi$_{0.2}$/SiO$_2$, (**d**) PtBi$_{0.3}$/SiO$_2$.
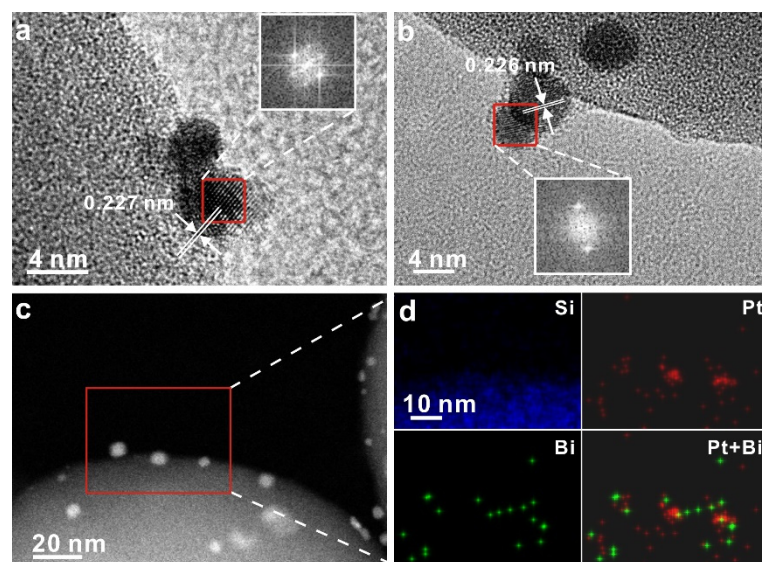

Figure 3. (**a**,**b**) HRTEM images of PtBi$_{0.2}$/SiO$_2$ catalyst (the insets show corresponding FFT patterns). (**c**) HAADF-STEM image and (**d**) EDS mapping of PtBi$_{0.2}$/SiO$_2$.
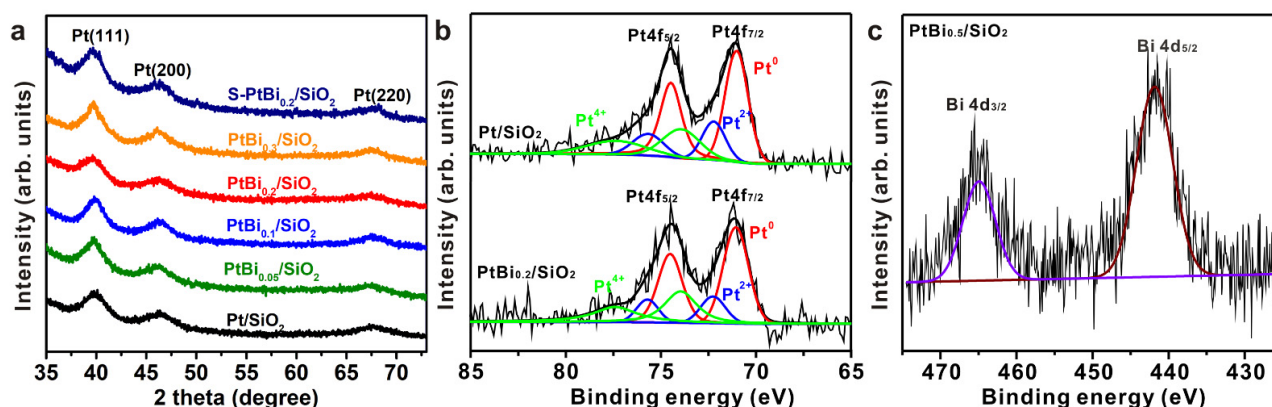
Figure 4. (**a**) XRD patterns of fresh and spent Pt/SiO$_2$ and PtBi$_x$/SiO$_2$ catalysts, the S-PtBi$_{0.2}$/SiO$_2$ (acquired after the 100-h long-term stability test); (**b**) Pt 4f XPS spectra of Pt/SiO$_2$ and PtBi$_{0.2}$/SiO$_2$; (**c**) Bi 4d XPS spectrum of PtBi$_{0.5}$/SiO$_2$.

X-ray photoelectron spectroscopy (XPS) was performed to explore the electronic structure of Pt and Bi of PtBi$_x$/SiO$_2$. Due to the very low concentration of Bi and the overlap of Si 2s, it is difficult to acquire a reliable Bi 4f spectrum for PtBi$_{0.2}$/SiO$_2$. However, once we increased the Bi loading to 0.5 wt.%, characteristic Bi 4d peaks at 464.9 and 441.8 eV could be observed, corresponding to Bi 4$d_{3/2}$ and Bi 4$d_{5/2}$ of Bi^{3+} [32,33]. It is reasonable that Bi species existed as Bi$_2$O$_3$ because the catalysts were pretreated in air before any characterizations and catalytic tests. The Pt 4f XPS spectrum of PtBi$_{0.2}$/SiO$_2$ was nearly consistent with that of Pt/SiO$_2$ (Figure 4b). After the reducing atmosphere (H$_2$/Ar) and the following air treatment, the valence state of Pt is very abundant, varying from 0 to +4. The relative content of Pt^0 calculated by peak area is also very similar to each other (56.0% for Pt/SiO$_2$ versus55.0% for PtBi$_{0.2}$/SiO$_2$). No significant shift of Pt 4f peaks corresponding to the electron transfer across Pt/Bi$_2$O$_3$ interface was observed, likely due to the relatively low concentration of Bi$_2$O$_3$ comparing with Pt. The signal of electron-rich Pt was likely overwhelmed by the signal of unaffected Pt and was therefore not observed by XPS.

To further investigate the electronic effects of bismuth oxides on Pt/SiO$_2$, we performed in situ diffuse reflectance infrared Fourier transform spectroscopy (DRIFTS) using CO as the probe molecule (Figure 5). The signals at 2050–2100 cm^{-1} can be assigned to linear CO adsorption on metallic Pt [34]. As for Pt/SiO$_2$, the frequency bands at 2088 and 2095 cm^{-1} originate from CO adsorbed on the terrace sites, and the weak shoulder band observed at 2075 cm^{-1} is assigned to CO adsorbed on the step sites of Pt [30,35]. With the introduction of 0.1 wt.% bismuth, one can find that both peaks move to the low frequency region. In addition, the relative intensity of band assigned to step sites adsorption also increases (blue line). When the bismuth amount increased to 0.2%, only one broad peak located at 2052 cm^{-1} is left and the stretching frequency is red-shifted by 12 cm^{-1} with respect to PtBi$_{0.1}$/SiO$_2$. Possible explanations include both geometric and electronic interactions between Pt and Bi$_2$O$_3$. The introduced bismuth species prefer to occupy the terrace sites of Pt which caused contribution of the assigned band gradually reduces as increased the content of Bi. At the same time, the introduced bismuth also acts as electron donor for Pt resulting the obvious red-shift of all the bands for linear CO adsorption. The observed electron effect of Bi is in good agreement with of the above theoretical calculations. The Bader charge of Pt on Bi$_2$O$_3$-Pt (111) is −0.168 |e| while that for Bi$_2$O$_3$ is +0.168 |e|, indicating creation of electron-rich Pt after Bi$_2$O$_3$ modification.
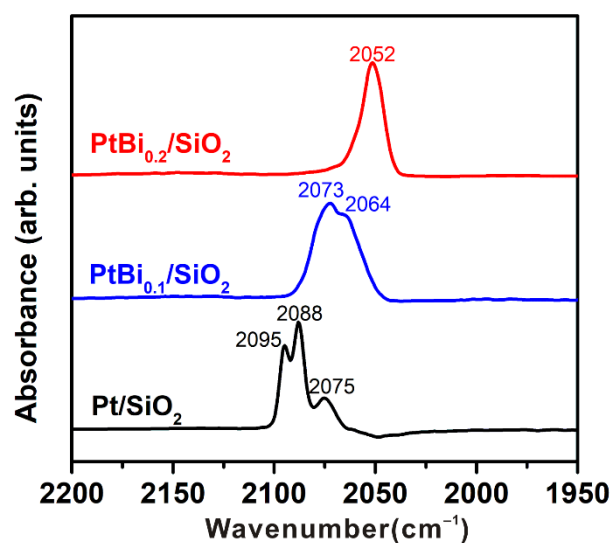
Figure 5. IR spectra of catalysts with pre-adsorbed CO.

Combination of both theoretical calculations and experimental characterizations revealed both geometric and electronic effects of small amount of Bi_2O_3 on the Pt structure, which might affect its catalytic performance as suggested by literatures [15,18,36]. The as-prepared $PtBi_x/SiO_2$ (x = 0–0.3) was then applied in the selective oxidative dehydrogenation of KA-oil. CO_2 is the main side-product in the current work. Other potential side-products are benzene, cyclohexene and 2-cyclohexanone and their total selectivity is negligible (less than 0.1%). As shown in Figure 6a, bare Pt/SiO_2 catalyst performed poor selectivity of cyclohexanone (only 16.2%) with 60.1% conversion of cyclohexanol. Interestingly, once bismuth was added, the selectivity of cyclohexanone was greatly improved. Specifically, when the loading of Bi increased from 0, 0.05, 0.1 to 0.2 wt.%, the cyclohexanone selectivity increased accordingly from 16.2%, 40.9%, 68.7% to 75.4%, respectively. It is important to note that in this range, the improvement of cyclohexanone selectivity does not compromise the cyclohexanol conversion. These results suggest that grafting small amount of Bi_2O_3 onto Pt surface will not geometrically block many active Pt sites. The geometric and electronic effect of these small amount of Bi_2O_3 are beneficial to the selective ODH of cyclohexanol. In contrast, once the loading of Bi reached 0.3 wt.%, although the cyclohexanone selectivity increased to 81.9%, the cyclohexanol conversion declined to 30.4%. This is likely due to the blocking of active Pt sites by excess Bi_2O_3. The inhabitation effect of bismuth on the catalytic activity also indicated that Bi_2O_3 itself is not reactive in this process. Taking together the conversion and selectivity data, the optimal Bi amount is 0.2 wt.% and is therefore adopted in the following study. Furthermore, we investigated the stability of $PtBi_{0.2}/SiO_2$ in the 100-h test as depicted in Figure 6b. Unlike Pt/SiO_2 which experienced 17.7% activity loss in our previous work [13], $PtBi_{0.2}/SiO_2$ exhibited excellent stable activity with a cyclohexanol conversion at about 56.2% to 63.4%. More importantly, we did not observe any obvious decrease of cyclohexanone selectivity. The catalytic test results here indicated that promotion effect of bismuth on Pt/SiO_2 catalyst system is stable and potential for industrial application. The XRD pattern of the spent $PtBi_{0.2}/SiO_2$ composite after the long-term test did not appear to have any new diffraction peaks, which verified the stability of the Pt-Bi system and good dispersion of Bi (Figure 4a).
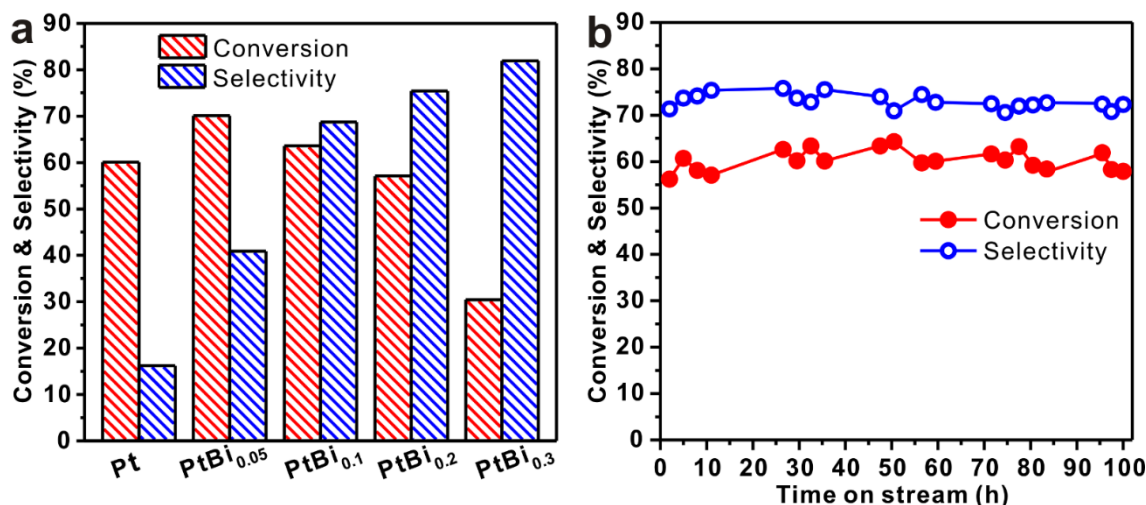
Figure 6. (**a**) Catalytic performances of Pt/SiO_2 and $PtBi_x/SiO_2$ in gas-phase ODH of KA-oil (mass ratio of alcohol and ketone is 1:1). (**b**) Long-term stability test of $PtBi_{0.2}/SiO_2$ catalyst. Reaction conditions: 180 °C, 0.2 g catalyst mixed with 1.2 g quartz sand, air = 16 mL min^{-1}, KA-oil = 0.4 mL h^{-1}. The carbon balance is >95%.

The promoting effect of bismuth towards the cyclohexanone selectivity is interesting and worth further investigation. As demonstrated before, the main byproduct in the catalytic process is CO_2. CO_2 could be produced by either cyclohexanol or cyclohexanone considering each of them account for 50 wt.% of the KA-oil substrate. The overoxidized cyclohexanone could come from the substrate, as well the as-generated one by cyclohexanol oxidation. Thus, studying the generation processes of CO_2 will indirectly shed light on the Bi promoting effect on the reaction mechanism. First, we applied Pt/SiO_2 and $PtBi_{0.2}/SiO_2$ in the gas-phase ODH of cyclohexanol to confirm whether the overoxidation of cyclohexanol dominates for the CO_2 generation. The conversion-selectivity relationship was obtained by carefully adjusting reaction conditions. As shown in Figure 7a, cyclohexanone selectivity decreased along with the increasing of conversion in both cases. One can notice that the red line ($PtBi_{0.2}/SiO_2$) is much higher than the black one (Pt/SiO_2) in the high-conversion area, which is in good line with the catalytic behavior in the ODH of KA-oil (Figure 6a). Considering that a large amount of ketone is generated when more than 50% alcohol converts, the selectivity difference between Pt/SiO_2 and $PtBi_{0.2}/SiO_2$ in low conversion degree is more persuasive for the investigation of CO_2 production. When the conversion of cyclohexanol is in low degree (<15%), cyclohexanone selectivity in both cases is higher than 88% whereas CO_2 production is limited, which indicated taht CO_2 generation from cyclohexanol could be reasonably excluded.
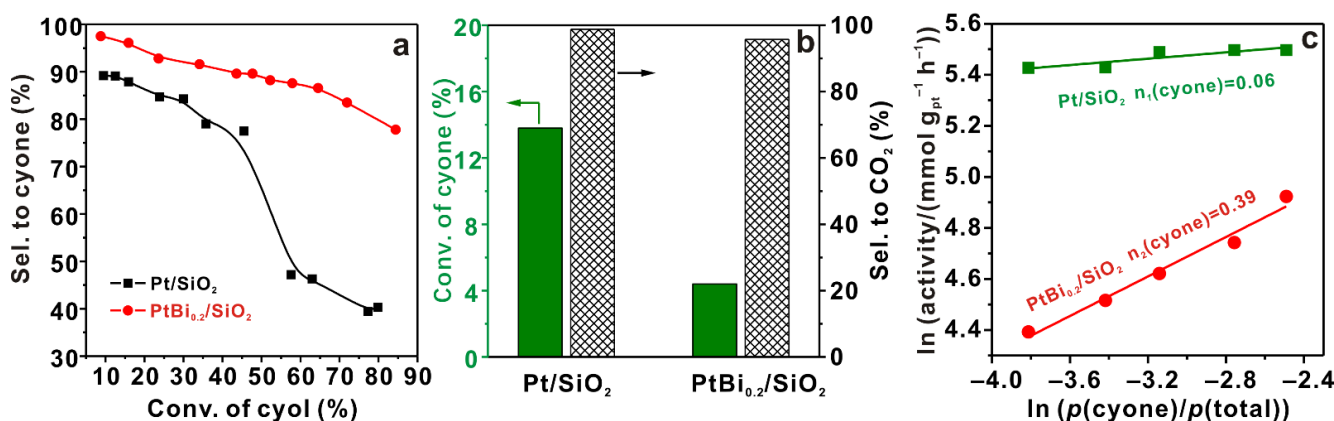
**Figure 7.** (**a**) Selectivity-conversion trajectories for Pt/SiO_2 and $PtBi_{0.2}/SiO_2$ catalysts in gas-phase ODH of cyclohexanol (cyol). (**b**) Catalytic activities of Pt/SiO_2 and $PtBi_{0.2}/SiO_2$ in total oxidation of cyclohexanone (cyone). (**c**) The influence of cyclohexanone partial pressure on catalytic activities of Pt/SiO_2 and $PtBi_{0.2}/SiO_2$ in total oxidation of cyclohexanone.

Second, we carried on experiments using cyclohexanone as the substrate to compare the overoxidation of cyclohexanone over Pt/SiO_2 and $PtBi_{0.2}/SiO_2$. As shown in Figure 7b, the cyclohexanone conversion over $PtBi_{0.2}/SiO_2$ was only one third of that over Pt/SiO_2 (4.4% versus 13.8%,), which provided solid evidence that overoxidation of ketone contributes to the CO_2 generation in the ODH of KA-oil greatly, and this reaction route was deeply inhibited by introduction of Bi_2O_3.

The possible explanation could be that Bi_2O_3 might weaken the adsorption ability of cyclohexanone on PtNPs and thus prevent cyclohexanone from being overoxidized. To explore the adsorption behavior of cyclohexanone, kinetic studies over Pt/SiO_2 and $PtBi_{0.2}/SiO_2$ were conducted in the total oxidation of cyclohexanone. In the cyclohexanone partial pressure test (Figure 7c), the apparent reaction order of cyclohexanone on Pt/SiO_2 and $PtBi_{0.2}/SiO_2$ is 0.06 and 0.39, respectively. The former value is similar to that of benzene [37] or o-xylene [38] in their complete combustion reaction catalyzed by Pt/Al_2O_3, which is quite close to zero. The smaller reaction order means stronger adsorption of ketone on Pt/SiO_2 comparing to $PtBi_{0.2}/SiO_2$. Furthermore, temperature-programmed desorption (TPD) of cyclohexanone was also measured on Pt/SiO_2 and $PtBi_{0.2}/SiO_2$. TPD curves in Figure 8 show three distinct desorption peaks. The one located at 160 °C is associated with the physical adsorption while the two located at high-temperature region origin from the chemisorbed species on the catalysts [13]. It is noted that the amount of chemisorption on Pt/SiO_2 is much more than that on $PtBi_{0.2}/SiO_2$. If we assume that all desorbed species are cyclohexanone, the chemisorbed amount of cyclohexanone on Pt/SiO_2 is 618 mg g_{Pt}^{-1}, whereas the adsorption amount on $PtBi_{0.2}/SiO_2$ reduces to 479 mg g_{Pt}^{-1}. Combination of the ketone partial pressure test and TPD results indicated that the added Bi greatly impaired the cyclohexanone adsorption ability of Pt/SiO_2, which is main factor of the improvement of the cyclohexanone selectivity by protecting is from overoxidation. The weak adsorption behavior of cyclohexanone originates from the geometric and electronic effects of bismuth and the resulting $Pt-Bi_2O_3$ interface as suggested in both characterizations and DFT calculations.
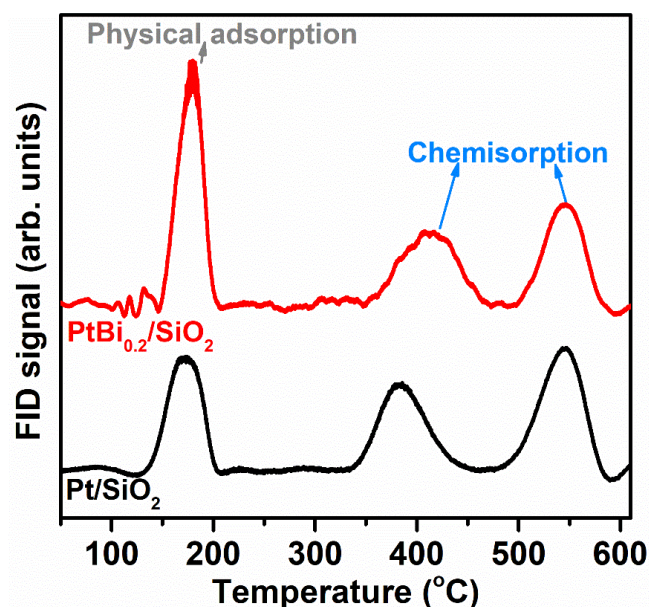

Figure 8. TPD curves of cyclohexanone on Pt/SiO_2 and $PtBi_{0.2}/SiO_2$.

3. Materials and Methods

3.1. Catalyst Preparation

3.1.1. Synthesis of Silica Nanospheres

The reagents used for SiO_2 synthesis were purchased from Sinopharm Chemical Reagent Co., Ltd. Shanghai, China. A previously reported Stöber method was applied

to synthesize spherical SiO_2 [39]. Typically, 6 mL of deionized water and 18 mL of 25% ammonium hydroxide aqueous solution were added into 360 mL of ethanol and stirred for 30 min at room temperature. Subsequently, 13.8 mL of tetraethyl orthosilicate was added, followed by vigorous stirring for 6 h. The mixture was centrifuged and washed with EtOH several times before being dried at 65 °C. Silica nanospheres were obtained after calcination at 400 °C for 5 h.

3.1.2. Synthesis of Pt Nanoparticles

Pt nanoparticles were synthesized according to the reference [28]. 133 mg of polyvinyl pyrrolidone (Aladdin Chemistry Co., Ltd., Shanghai, China) and 20 mL of 6 mM $H_2PtCl_6 \cdot H_2O$ solution (Macklin Biochemical Co., Ltd., Shanghai, China) were added into 180 mL ethanol, followed by reflux for 3 h. The solution was then redispersed in deionized water after rotatory evaporation until no ethanol was left.

3.1.3. Preparation of Pt/SiO_2 and $PtBi_x/SiO_2$

The loading amount of Pt was fixed as 1 wt.% for all samples. X was the mass ratio of Bi to Pt which varied from 0.05 to 0.3. In a typical preparation process, certain amount of bismuth nitrate and the previously prepared Pt colloidal solution were dissolved in water before the addition of SiO_2 nanospheres. The mixture was continuously stirred at 60 °C until the water totally dried. The acquired products were calcined at 400 °C for 5 h in 5% H_2/Ar and then 250 °C for 2 h in air.

3.2. Catalyst Characterization

X-ray diffraction (XRD) patterns were recorded on a Rigaku Ultimate IV diffractometer (Rigaku, Tokyo, Japan) using Cu Kα radiation (40 kV, 40 mA). Transmission electron microscopy (TEM) images were collected on a FEI Tecnai G2 F20 S-TWIN microscope (FEI, Hillsboro, OR, USA) and a Hitachi HT-7700 microscope (Hitachi, Tokyo, Japan). High angle annular dark field scanning transmission electron microscopy (HAADF-STEM) was carried out on a FEI Titan ChemiSTEM (FEI, Hillsboro, OR, USA) operated at 200 kV. X-ray photoelectron spectroscopy (XPS) was performed in a Thermo Scientific K-Alpha+ spectrometer (Thermo Scientific, Waltham, MA, USA). In situ Fourier transform infrared (FT-IR) adsorption spectroscopy experiments (Thermo Scientific, Waltham, MA, USA) were conducted by using CO as probe molecule and was recorded on a Nicolet iS50 instrument at room temperature. Typically, 100 mg of samples were pretreated in N_2 at 200 °C for 1 h and then cooled down to room temperature before a background spectrum was collected. A CO flow was introduced into the sample pool for 30 min followed by a flush of N_2 flow to desorb most of the physically adsorbed CO. IR spectra was collected till the signals remained unchanged. The temperature-programmed desorption (TPD) of cyclohexanone were performed on a home-made machine using N_2 as the carrier gas. The desorbed species was detected by a flame ionization detector(Shanghai Kexiao Technology Instrument Co., LTD, Shanghai, China). Typically, 50 mg of samples was pretreated by cyclohexanone at 165 °C for 1 h and then flushed by a N_2 flow to remove the weakly adsorbed species. After the temperature cooled down to room temperature, the TPD data were collected at a heating rate of 5 °C min^{-1} to 650 °C. The adsorption amount of cyclohexanone is calculated by an external standard method.

3.3. Catalytic Measurement

The gas-phase oxidative dehydrogenation (ODH) of KA-oil (50 wt% cyclohexanol and 50 wt% cyclohexanone) was performed in a glass fixed-bed tube reactor with an inner diameter of 12 mm under atmospheric pressure. Standard air was used as oxidant and the flow rate was set at 16 mL min^{-1}. The liquid reagent was supplied through a syringe pump (0.4 mL h^{-1}) and was gasified on the reactor wall before the catalytic bed at 180 °C. The products were collected at reaction equilibrium after running for 1.5 h. The condensed liquid-phase products were analyzed by GC equipped with a flame ionization detector

using triethylene glycol dimethyl ether as internal standard. CO_2 was the only gas-phase product and was analyzed by GC equipped with a thermal conductivity detector. The ODH of cyclohexanol and cyclohexanone tests were similar to the process mentioned above. The catalysts (10–200 mg) were mixed with quartz sand before loading. Flow rate of air varied from 16 to 48 mL min^{-1} and that of liquid reactants is 0.2–0.6 mL h^{-1}. As for partial pressure experiment of cyclohexanone oxidation, O_2 partial pressure was fixed. The partial pressure of cyclohexanone was adjusted by charging rate of the liquid flow rate while N_2 was used as balance gas. In all cases, the carbon balance was >95%.

3.4. DFT Calculations

The Vienna Ab-initio Simulation Package (VASP) was applied for the density functional theory (DFT) calculations [40]. Spin-polarized projector augmented wave (PAW) method [41] and Perdew–Burke–Ernzerhof (PBE) [42] electron exchange-correlation function of the generalized gradient approximation (GGA) [43] were used. The kinetic energy cut-off for the wave function expanded in the plane-wave basis was set as 400 eV. The vacuum height was set as 15 Å to eliminate the interaction between neighboring slabs.

The adsorption energy (E_{ads}) was calculated as follows:

$$E_{ads} = - (E_{total} - E_{substrate} - E_{gas\text{-}phase\ adsorbate}) \tag{1}$$

where $E_{substrate}$ is the energy of the clean substrate, E_{total} is the calculated total energy of the adsorption system, and $E_{gas\text{-}phase\ adsorbate}$ is the energy of the gas-phase molecule.

The structure of Bi_2O_3-Pt(111) was built by the genetic algorithm optimization method inside the USPEX crystal structure prediction software, which has been successfully applied in the prediction of stable structure of massive crystals, nanoclusters, and reconstructed crystal surfaces [26,27]. A 4×4 surface cell was used to construct a four-layer Pt(111) slab, the top two layers of the Pt(111) were allowed to relax. At the same time, other atoms (bottom two layers) were fixed, and each possible structure was allowed to relax until the maximum force was less than 0.05 eVÅ^{-1}. The Brillouin-zone integration was performed along with a $2 \times 2 \times 1$ Monkhorst-Pack grid for the different surface slabs.

4. Conclusions

In short, we successfully designed and synthesized a Bi_2O_3 modified Pt/SiO_2 catalyst directed by the theoretical calculations. Characterizations displayed that the introduced small amount of Bi_2O_3 barely blocked the active sites of Pt but can donate electrons to Pt. The $PtBi_{0.2}/SiO_2$ exhibited a 5 times higher cyclohexanone selectivity than Pt/SiO_2 at the same conversion of cyclohexanol in the selective oxidation of KA-oil with excellent stability. Experimental results revealed that the engineered Pt-Bi_2O_3 interfaces help to weaken the adsorption of cyclohexanone, which effectively prevents the latter from being over-oxidized and thus leads to outstanding catalytic performances. The outcome of the current work paves a new way to optimize the adsorption capability for the noble metal catalysts for the structure-sensitive reactions and enriches our understanding of promoting effects of bismuth.

Author Contributions: Q.Z.: Investigation, data curation, visualization, writing—original draft preparation; Z.-Q.W.: Theoretical calculation data curation, formal analysis; W.H.: Investigation, data curation; B.L.: Data curation, formal analysis; S.Z.: writing—review and editing, supervision, project administration, funding acquisition. All authors have read and agreed to the published version of the manuscript.

Data Availability Statement: The data presented in this study are available on request from the corresponding author.

References

1. Liu, H.; Jiang, T.; Han, B.; Liang, S.; Zhou, Y. Selective Phenol Hydrogenation to Cyclohexanone Over a Dual Supported Pd–Lewis Acid Catalyst. *Science* **2009**, *326*, 1250–1252. [CrossRef]
2. Li, Z.L.; Liu, J.H.; Xia, C.G.; Li, F.W. Nitrogen-Functionalized Ordered Mesoporous Carbons as Multifunctional Supports of Ultrasmall Pd Nanoparticles for Hydrogenation of Phenol. *ACS Catal.* **2013**, *3*, 2440–2448. [CrossRef]
3. Dugal, M.; Sankar, G.; Raja, R.; Thomas, J.M. Designing a Heterogeneous Catalyst for the Production of Adipic Acid by Aerial Oxidation of Cyclohexane. *Angew. Chem. Int. Ed.* **2000**, *39*, 2310–2313. [CrossRef]
4. Fridman, V.Z.; Davydov, A.A. Dehydrogenation of Cyclohexanol on Copper-Containing Catalysts I. The Influence of the Oxidation State of Copper on the Activity of Copper Sites. *J. Catal.* **2000**, *195*, 20–30. [CrossRef]
5. Nagaraja, B.M.; Kumar, V.S.; Shashikala, V.; Padmasri, A.H.; Reddy, S.S.; Raju, B.D.; Rao, K.S.R. Effect of Method of Preparation of Copper-Magnesium Oxide Catalyst on the Dehydrogenation of Cyclohexanol. *J. Mol. Catal. A Chem.* **2004**, *223*, 339–345. [CrossRef]
6. Tan, K.; Fujiii, K.; Nakamura, M.; Hanada, K. Process for Removing Impurities from the Mixture of Cyclohexanone and Cyclohexanol. U.S. Patent US5168983(A), 22 March 1991.
7. Becker, C.L.; Davis, J.D.; Dakka, J.M.; Nadler, K.C. Process for Making Cyclohexanone. U.S. Patent US2017283353(A1), 8 September 2015.
8. Gill, A.M.; Hinde, C.S.; Leary, R.K.; Potter, M.E.; Jouve, A.; Wells, P.P.; Midgley, P.A.; Thomas, J.M.; Raja, R. Design of Highly Selective Platinum Nanoparticle Catalysts for the Aerobic Oxidation of KA-Oil using Continuous-Flow Chemistry. *ChemSusChem* **2016**, *9*, 423–427. [CrossRef]
9. Valente, A.; Lin, Z.; Brandao, P.; Portugal, I.; Anderson, M.; Rocha, J. Gas-phase Oxidative Dehydrogenation of Cyclohexanol over ETS-10 and Related Materials. *J. Catal.* **2001**, *200*, 99–105. [CrossRef]
10. Zhao, G.F.; Yang, F.; Chen, Z.J.; Liu, Q.F.; Ji, Y.J.; Zhang, Y.; Niu, Z.Q.; Mao, J.J.; Bao, X.H.; Hu, P.J.; et al. Metal/Oxide Interfacial Effects on the Selective Oxidation of Primary Alcohols. *Nat. Commun.* **2017**, *8*, 14039–14046. [CrossRef]
11. Yi, W.; Yuan, W.; Meng, Y.; Zou, S.; Zhou, Y.; Hong, W.; Che, J.; Hao, M.; Ye, B.; Xiao, L.; et al. A Rational Solid-State Synthesis of Supported Au-Ni Bimetallic Nanoparticles with Enhanced Activity for Gas-Phase Selective Oxidation of Alcohols. *ACS Appl. Mater. Interfaces* **2017**, *9*, 31853–31860. [CrossRef]
12. Santhanaraj, D.; Suresh, C.; Vijayan, P.; Venkatathri, N.; Shanthi, K. Mn-MCM-41 Molecular Sieves: A Selective Gas-Phase Cyclohexanol Oxidation Catalyst. *React. Kinet. Mech. Catal.* **2010**, *99*, 439–446. [CrossRef]
13. Hong, W.; Wang, Z.-Q.; Zou, S.; Zhou, Y.; Lu, L.; Zhou, Q.; Gong, X.-Q.; Fan, J. Calcination Atmosphere Regulated Morphology and Catalytic Performance of Pt/SiO$_2$ in Gas-phase Oxidative Dehydrogenation of KA-oil. *ChemCatChem* **2018**, *10*, 5689–5697. [CrossRef]
14. Chen, G.; Xu, C.; Huang, X.; Ye, J.; Gu, L.; Li, G.; Tang, Z.; Wu, B.; Yang, H.; Zhao, Z.; et al. Interfacial Electronic Effects Eontrol the Reaction Selectivity of Platinum Catalysts. *Nat. Mater.* **2016**, *15*, 564–569. [CrossRef] [PubMed]
15. Lou, B.; Kang, H.; Yuan, W.; Ma, L.; Huang, W.; Wang, Y.; Jiang, Z.; Du, Y.; Zou, S.; Fan, J. Highly Selective Acetylene Semihydrogenation Catalyst with an Operation Window Exceeding 150 °C. *ACS Catal.* **2021**, *11*, 6073–6080. [CrossRef]
16. Zhou, Y.; Zhu, Y.; Wang, Z.Q.; Zou, S.; Ma, G.; Xia, M.; Kong, X.; Xiao, L.; Gong, X.Q.; Fan, J. Catalytic Activity Control via Crossover between Two Different Microstructures. *J. Am. Chem. Soc.* **2017**, *139*, 13740–13748. [CrossRef]
17. Mallat, T.; Bodnar, Z.; Hug, P.; Baiker, A. Selective Oxidation of Cinnamyl Alcohol to Cinnamaldehyde with Air over Bi-Pt/Alumina Catalysts. *J. Catal.* **1995**, *153*, 131–143. [CrossRef]
18. Villa, A.; Wang, D.; Veith, G.M.; Prati, L. Bismuth as a Modifier of Au–Pd Catalyst: Enhancing Selectivity in Alcohol Oxidation by Suppressing Parallel Reaction. *J. Catal.* **2012**, *292*, 73–80. [CrossRef]
19. Yan, Y.; Ye, B.; Chen, M.; Lu, L.; Yu, J.; Zhou, Y.; Wang, Y.; Liu, J.; Xiao, L.; Zou, S.; et al. Site-specific Deposition Creats Electron-Rich Pd Atoms for Unprecedented C-H Activation in Aerobic Alcohol Oxidation. *Chin. J. Catal.* **2020**, *41*, 1240–1247. [CrossRef]
20. Liu, L.; Li, H.; Tan, Y.; Chen, X.; Lin, R.; Yang, W.; Huang, C.; Wang, S.; Wang, X.; Liu, X.Y.; et al. Metal-Support Synergy of Supported Gold Nanoclusters in Selective Oxidation of Alcohols. *Catalysts* **2020**, *10*, 107. [CrossRef]
21. Liu, J.; Zou, S.; Wu, J.; Kobayashi, H.; Zhao, H.; Fan, J. Green Catalytic Oxidation of Benzyl Alcohol over Pt/ZnO in Base-Free Aqueous Medium at Room Temperature. *Chin. J. Catal.* **2018**, *39*, 1081–1089. [CrossRef]
22. Liu, J.; Han, F.; Chen, L.; Lu, L.; Zou, S.; Zhao, H. Remarkable Promoting Effects of BiOCl on the Room-Temperature Selective Oxidation of Benzyl Alcohol over Supported Pt Catalysts. *New J. Chem.* **2018**, *42*, 8979–8984. [CrossRef]
23. Mondelli, C.; Grunwaldt, J.-D.; Ferri, D.; Baiker, A. Role of Bi Promotion and Solvent in Platinum-Catalyzed Acohol Oxidation Probed by in Situ X-ray Absorption and ATR-IR Spectroscopy. *Phys. Chem. Chem. Phys.* **2010**, *12*, 5307–5316. [CrossRef]
24. Mallat, T.; Bodnar, Z.; Baiker, A.; Greis, O.; Strubig, H.; Reller, A. Preparation of Promoted Platinum Catalysts of Designed Geometry and the Role of Promoters in the Liquid-Phase Oxidation of 1-Methoxy-2-propanol. *J. Catal.* **1993**, *142*, 237–253. [CrossRef]
25. Zhou, C.; Guo, Z.; Dai, Y.; Jia, X.; Yu, H.; Yang, Y. Promoting Role of Bismuth on Carbon Nanotube Supported Platinum Catalysts in Aqueous Phase Aerobic Oxidation of Benzyl Alcohol. *Appl. Catal. B Environ.* **2016**, *181*, 118–126. [CrossRef]
26. Oganov, A.R.; Lyakhov, A.O.; Valle, M. How Evolutionary Crystal Structure Prediction Works—And Why. *Acc. Chem. Res.* **2011**, *44*, 227–237. [CrossRef]

27. Wang, Q.; Oganov, A.R.; Zhu, Q.; Zhou, X.-F. New Reconstructions of the (110) Surface of Rutile TiO$_2$ Predicted by an Evolutionary Method. *Phys. Rev. Lett.* **2014**, *113*, 266101. [CrossRef]

28. Teranishi, T.; Hosoe, M.; Tanaka, T.; Miyake, M. Size Control of Monodispersed Pt Nanoparticles and Their 2D Organization by Electrophoretic Deposition. *J. Phys. Chem. B* **1999**, *103*, 3818–3827. [CrossRef]

29. Liu, S.; Tian, N.; Xie, A.-Y.; Du, J.-H.; Xiao, J.; Liu, L.; Sun, H.-Y.; Cheng, Z.-Y.; Zhou, Z.-Y.; Sun, S.-G. Electrochemically Seed-Mediated Synthesis of Sub-10 nm Tetrahexahedral Pt Nanocrystals Supported on Graphene with Improved Catalytic Performance. *J. Am. Chem. Soc.* **2016**, *138*, 5753–5756. [CrossRef]

30. Ning, X.; Li, Y.; Yu, H.; Peng, F.; Wang, H.; Yang, Y. Promoting Role of Bismuth and Antimony on Pt Catalysts for the Selective Oxidation of Glycerol to Dihydroxyacetone. *J. Catal.* **2016**, *335*, 95–104. [CrossRef]

31. Huang, Y.; Cai, J.; Guo, Y. A High-Efficiency Microwave Approach to Synthesis of Bi-Modified Pt Nanoparticle Catalysts for Ethanol Electro-Oxidation in Alkaline Medium. *Appl. Catal. B Environ.* **2013**, *129*, 549–555. [CrossRef]

32. Nyholm, R.; Berndtsson, A.; Martensson, N. Core Level Binding Energies for the Elements Hf to Bi (Z = 72–83). *J. Phys. C Solid State Phys.* **1980**, *13*, L1091–L1096. [CrossRef]

33. Hou, D.; Hu, X.; Hu, P.; Zhang, W.; Zhang, M.; Huang, Y. Bi$_4$Ti$_3$O$_{12}$ nanofibers–BiOI nanosheets p–n junction: Facile synthesis and enhanced visible-light photocatalytic activity. *Nanoscale* **2013**, *5*, 9764–9772. [CrossRef]

34. Borchert, H.; Fenske, D.; Kolny-Olesiak, J.; Parisi, J.; Al-Shamery, K.; Bäumer, M. Ligand-Capped Pt Nanocrystals as Oxide-Supported Catalysts: FTIR Spectroscopic Investigations of the Adsorption and Oxidation of CO. *Angew. Chem. Int. Ed.* **2007**, *46*, 2923–2926. [CrossRef] [PubMed]

35. Hollins, P. The Influence of Surface Defects on the Infrared Spectra of Adsorbed Species. *Surf. Sci. Rep.* **1992**, *16*, 51–94. [CrossRef]

36. Xie, J.; Huang, B.; Yin, K.; Pham, H.N.; Unocic, R.R.; Datye, A.K.; Davis, R.J. Influence of Dioxygen on the Promotional Effect of Bi during Pt-Catalyzed Oxidation of 1, 6-Hexanediol. *ACS Catal.* **2016**, *6*, 4206–4217. [CrossRef]

37. Morales-Torres, S.; Pérez-Cadenas, A.F.; Kapteijn, F.; Carrasco-Marín, F.; Maldonado-Hódar, F.J.; Moulijn, J.A. Palladium and Platinum Catalysts Supported on Carbon Nanofiber Coated Monoliths for Low-Temperature Combustion of BTX. *Appl. Catal. B Environ.* **2009**, *89*, 411–419. [CrossRef]

38. Manta, C.M.; Bozga, G.; Bercaru, G.; Bîldea, C.S. Kinetics of o-Xylene Combustion over a Pt/Alumina Catalyst. *Chem. Eng. Technol.* **2012**, *35*, 2147–2154. [CrossRef]

39. Stöber, W.; Fink, A.; Bohn, E. Controlled growth of monodisperse silica spheres in the micron size range. *J. Colloid Interface Sci.* **1968**, *26*, 62–69. [CrossRef]

40. Kresse, G.; Furthmüller, J. Efficient iterative schemes for ab initio total-energy calculations using a plane-wave basis set. *Phys. Rev. B* **1996**, *54*, 11169–11186. [CrossRef]

41. Blöchl, P.E. Projector Augmented-Wave Method. *Phys. Rev. B* **1994**, *50*, 17953–17979. [CrossRef] [PubMed]

42. Perdew, J.P.; Burke, K.; Ernzerhof, M. Generalized Gradient Approximation Made Simple. *Phys. Rev. Lett.* **1996**, *77*, 3865–3868. [CrossRef]

43. Teter, M.P.; Payne, M.C.; Allan, D.C. Solution of Schrödinger's Equation for Large Systems. *Phys. Rev. B* **1989**, *40*, 12255–12263. [CrossRef] [PubMed]